Available online at www.sciencedirect.com
ScienceDirect
Journal of Power Sources 172 (2007) 395–403
JOURNAL OF POWER SOURCES
www.elsevier.com/locate/jpowsour

Butylene sulfite as a film-forming additive to propylene carbonate-based electrolytes for lithium ion batteries

Renjie Chen [a,b], Feng Wu [b,*], Li Li [b], Yibiao Guan [b], Xinping Qiu [a], Shi Chen [b], Yuejiao Li [b], Shengxian Wu [b]

[a] *Department of Chemistry, Tsinghua University, Beijing 100084, China*
[b] *School of Chemical Engineering & the Environment, Beijing Institute of Technology, Beijing 100081, China*

Received 20 July 2006; received in revised form 26 April 2007; accepted 21 May 2007
Available online 25 May 2007

Abstract

Butylene sulfite (BS) has been synthesized and the BS-based electrolytes containing different lithium salt are evaluated with differential scanning calorimetry (DSC) and alternating current impedance spectroscopy. These electrolytes exhibit high thermal stability and good electrochemical properties. BS has been investigated as a new film-forming additive to propylene carbonate (PC)-based electrolytes for use in lithium ion batteries. Even in small additive amounts (5 vol.%) BS can effectively suppress the co-intercalation of PC with solvation lithium ion into graphite. The formation of a stable passivating film on the graphite surface is believed to be the reason for the improved cell performance. The LUMO energy and the total energy of the sulfite molecules are higher than that of the carbonate ones. It is clearly indicated that the sulfite molecules can easily accept electrons and bears a high reaction activity. The lithium-oxy-sulfite film (Li_2SO_3 and $ROSO_2Li$) resulting from the reductive decomposition of BS is studied by the density functional theory (DFT) calculations. In addition, the PC-BS electrolytes are characterized by a high oxidation stability allowing the cycling of a $LiMn_{1.99}Ce_{0.01}O_4$ and $LiFePO_4$-C cathodes with good reversibility.

Keywords: Lithium ion battery; Electrolyte additive; Butylene sulfite; Graphite; Solid electrolyte interphase

1. Introduction

The development of new electrolytes has attracted considerable attention in electrochemical field in order to improve battery performance [1,2]. Due to the growing use of portable electronic devices and electric vehicles (EVs), lithium ion batteries are undergoing rapid development aimed at higher energy density, higher power density and cycling stability [3,4]. With such excellent properties as low melting point (224.2 K), high boiling point (514.9 K), high flash point (405.2 K), high dielectric constant, high chemical stability toward metallic lithium and wide electrochemical window, propylene carbonate (PC) is an attractive candidate as solvent for nonaqueous electrolytes in the lithium ion batteries at both high and low temperatures and is also helpful in improving the safety of the lithium ion batteries. Graphite is widely used as anode materials for lithium ion batteries due to its low cost and high capacity as well as low and flat potential plateau in respect to lithium metal. However, graphite is highly sensitive to electrolyte solutions, especially to PC-based electrolytes, because electrolyte solvents and solvated Li^+ ions tend to cointercalate into graphite [5]. This leads to severe exfoliation of the graphite layers and destruction of the graphite structure. Because the intercalation of lithium into graphite occurs at low potentials (below 0.25 V versus Li/Li^+), the relevant solvents and salts are partially reduced to form solid electrolyte interphase (SEI) on the surface of graphite electrodes. The formation of SEI is associated with the irreversible capacity loss. And the properties of the SEI film play a crucial role in the battery performance, including cycle life, self-discharge, coulombic efficiency and irreversible capacity. Therefore, many methods have been developed to suppress solvent co-intercalation into graphite. One effective method is the employment of film-forming electrolyte additives that predominantly react on the graphite electrode surfaces during the first cycling process. It was reported that the common additives are CO_2 [6], SO_2 [7], halogenated ester [8] or carbonate [9] and vinylene compound [3,10,11].

* Corresponding author. Tel.: +86 10 68912508; fax: +86 10 68451429.
E-mail address: wufeng863@vip.sina.com (F. Wu).

0378-7753/$ – see front matter © 2007 Elsevier B.V. All rights reserved.
doi:10.1016/j.jpowsour.2007.05.078

As a novel solvent and electrolyte additive, sulfites have attracted increasing attention. Winter et al. [12–14] have reported on the use of the cyclic organic sulfites ethylene sulfite (ES) and propylene sulfite (PS) as film-forming electrolyte additives for lithium ion batteries with graphitic anodes. Small amounts of the cyclic sulfites (typically 5 vol.%) added to PC-based electrolytes improved the anode behavior significantly because PC co-intercalation into graphite is suppressed or even avoided. Subsequently, several papers, which focused on electrochemical application with ES or PS as electrolyte additive, have been reported [15–19].

In this paper, a new sulfite solvent, butylene sulfite (BS), was synthesized and investigated as a film-forming additive for nonaqueous electrolyte-based lithium ion batteries. It was found that the addition of BS allows the successful use of graphite anodes and of the $LiMn_{1.99}Ce_{0.01}O_4$ and $LiFePO_4$-C cathodes in PC-based electrolyte. Meanwhile, a detailed study of the film resulting from the reductive decomposition of BS by the density function theory (DFT) calculations was performed.

2. Experimental

The synthetic methods for BS had been reported in literature [20–22]. However, direct synthesis with protochloride sulfone and butanediol by following reaction was found to give equally good results (Fig. 1).

BS and PC (Beijing Phylion Battery Company, battery grade) were distilled under vacuum. The solvents were stored over 4 Å molecular sieves under high purity argon. $LiN(SO_2CF_3)_2$, (LiTFSI) (3M Inc., 99%), $LiCF_3SO_3$ (Acros, 99%) and $LiClO_4$ (Acros, AP) were dried at 140 °C for 12 h in vacuum.

The graphite electrodes were prepared from 85 wt.% MCMB (Shanghai Shanshan Company, battery grade) and 10 wt.% carbon black by using slurry of carbon material with a solution of 5 wt.% Polyvinylidene Fluoride (PVDF) dissolved in *N*-methyl-2-pyrrolidinone (NMP). The slurry was cast onto copper foil and then dried at 120 °C for 12 h, then pressed at 8 MPa, and finally dried under vacuum at 55 °C for 6 h again and cut to 8 mm × 8 mm in size. $LiMn_{1.99}Ce_{0.01}O_4$-based cathodes were made from 85 wt.% $LiMn_{1.99}Ce_{0.01}O_4$ active material that was synthesized by solid state reaction, 10 wt.% acetylene black and 5 wt.% PVDF. Similarly, $LiFePO_4$-C composite electrode were made from 75 wt.% $LiFePO_4$-C active material that was synthesized by solid state reaction, 20 wt.% acetylene black and 5 wt.% PVDF. The preparations of the cathodes were carried out as described for the anodes. However, instead of copper foil, aluminium foil was used as current collector. Electrolyte preparation and cell assembly were accomplished in an argon-filled MBraun LabMaster 130 glove box ($H_2O < 5$ ppm). The water content of the electrolytes was determined to be less than 25 ppm by the Karl–Fischer titration method on DL37KF coulometer, Mettler Toledo.

The melting point and boiling point of BS and the thermal properties of BS-based electrolytes were determined on a DSC 2010 differential scanning calorimeter (TA Inc.) by sealing ca. 10 mg of the sample in an aluminum pan. The pan and the electrolyte were first cooled to about −100 °C with liquid nitrogen and then heated to 300 °C at a rate of 5 °C min^{-1}. Special attention was paid to avoid exposing the hygroscopic samples to moisture by continuous nitrogen flowing around the sample during measurement. Ionic conductivity measurements were carried out with an electrochemical cell with Pt electrode. The cell constant was determined with standard KCl solution (0.01 M) at 25 °C. The AC impedance of the samples was measured on a CHI660a electrochemical workstation (1 Hz to 100 KHz, −30 to 80 °C). The constant current charge–discharge experiments were carried out on a Land cell tester using a two-electrode cell. The cyclic voltammetry (CV) measurements were performed on a CHI660a electrochemical workstation with either graphite or cathodes electrode as the working electrodes and lithium foil (99.9%) as the counter and reference electrodes. All the cells were assembled under a dry argon atmosphere in the glove box.

The molecular structures of the organic carbonates and sulfites were optimized with the BLYP function of nonlocal DFT with DNP basis set using the DMol3 module of the Cerius2 program. The total energy and frontier molecular orbital energy of each organic molecule are calculated with this program. The equilibrium and transition structures of the reductive dissociation process of BS were fully optimized at the same level. The sizes of the DNP basis sets are comparable to the Gaussian 6-31G** basis sets, giving the p polarization functions on hydrogen apart form the d functions on the heavy atoms. In particular, the numerical basis set is much more accurate than a Gaussian basis set of the same size [23].

3. Results and discussion

3.1. Thermal properties and ionic conductivities

Fig. 2 shows the typical DSC trace of the phase transitions during the heating scans from −100 to 230 °C for pure BS. It shows the changes of the heat capacities corresponding to the melting point (T_m, −23 °C), together with a sharp endothermic peak at 212 °C corresponding to the boiling point (T_b). This

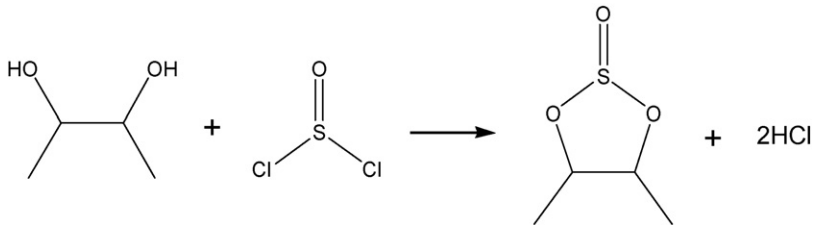

Fig. 1. Synthetic reaction of butylene sulfite.

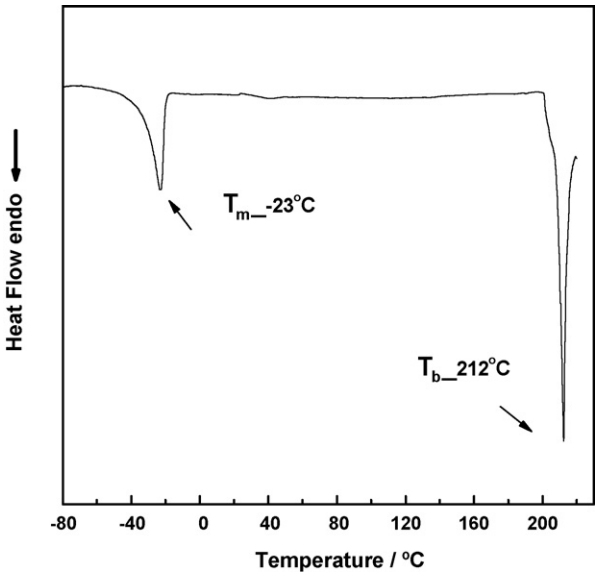

Fig. 2. DSC curve for butylene sulfite.

indicates that the butylene sulfite own a wide liquid range. Furthermore, the thermal properties of BS-based electrolytes with different lithium salt, 1 M LiTFSI/BS, 1 M $LiCF_3SO_3$/BS and 1 M $LiClO_4$/BS, are evaluated with DSC. It is worth noticing that none endothermic or exothermic peak is observed in the temperature range of −100 to 180 °C. This means that these electrolytes possess the good low temperature performance and high thermal stability in the studied temperature range.

PC electrolytes are known for their better low temperature behavior and remain effective conductivity even at temperatures <−30 °C. Looking at the conductivities of PC and PC/BS (95:5 by volume) electrolytes in Fig. 3, there is a neglectable discrepancy at each temperature. It is feasible that BS is used as an additive in small amounts from the viewpoint of the ionic conductivity. Similar to the carbonate-based electrolyte solutions (e.g. in PC and ethylene carbonate (EC)), the three BS-based electrolytes show the high ionic conductivity.

The conductivity–temperature data of 1 M $LiClO_4$ in BS plotted in the Arrhenius coordinated show a linear profile

Table 1
Ionic conductivities of the BS-based electrolyte containing various salts and 1 M $LiClO_4$/PC:BS (95:5 by volume)

	Ionic Conductivity (mS cm^{-1})			
	−30 °C	0 °C	25 °C	50 °C
1 M LiTFSI/BS	0.73	2.34	3.92	5.67
1 M $LiCF_3SO_3$/BS	0.08	0.27	0.51	0.80
1 M $LiClO_4$/BS	0.29	1.08	2.05	3.19
1 M $LiClO_4$/PC:BS (95:5 by volume)	0.62	2.46	4.55	7.27

(Fig. 3, inset), indicating that their conductivity–temperature relationships follow the Arrhenius equation due to low viscosity. Of all the BS-based electrolytes, the 1 M LiTFSI in BS shows the highest ionic conductivity at the same temperatures, which is 3.92×10^{-3} S cm^{-1} at room temperature and rises to 5.67×10^{-3} S cm^{-1} at 50 °C (Table 1).

3.2. Charge–discharge tests

It is well known that PC and the solvated Li^+ ions can co-intercalate into graphite at a potential of ca. 0.9 V versus Li/Li^+ and the electrode potential cannot reach the potential value (<0.2 V versus Li/Li^+) for intercalation of unsolvated Li^+ ions. It can be seen that there is no lithium intercalation plateau except for a long discharge plateau at ca. 0.8 V for the curve (a) in Fig. 4, suggesting that the SEI cannot form on the MCMB electrode in the PC-based electrolyte without an additive. Graphites exfoliate rapidly due to massive cointercalation and decomposition of PC ending commonly in electrode destruction. Continuous exfoliation of graphite leads to delamination of the active materials from the current collector and it goes along with the reduction of the working electrode.

In contrast, the addition of 5 vol.% BS greatly suppressed solvent co-intercalation and the exfoliation of graphite. The curve (b) in Fig. 4 corresponds to the voltage-capacity profile of the first two cycles of graphite/Li cell using 1 M $LiClO_4$ PC/BS (95:5 by volume) as electrolyte. Owing to the addition of BS, the voltage profile of graphite/Li cell changed completely. The cell

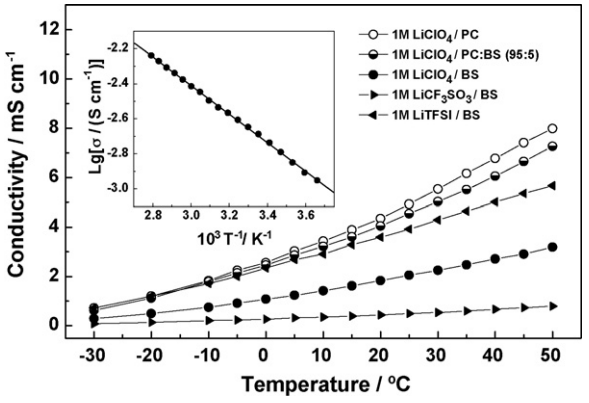

Fig. 3. Conductivity vs. temperature diagrams of PC-based and BS-based electrolytes. (Inset) The Arrhenius plots of conductivity for 1 M $LiClO_4$/BS electrolyte.

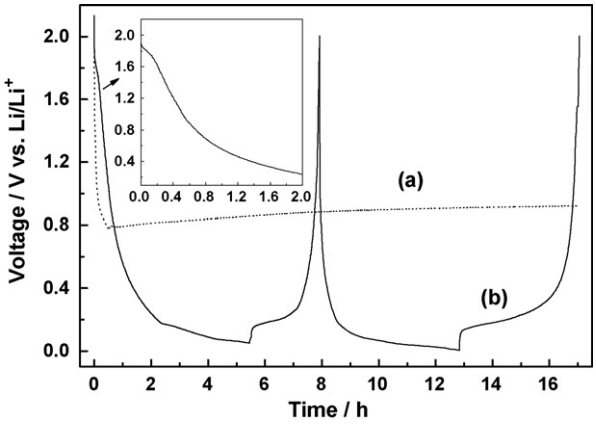

Fig. 4. First and second charge/discharge cycles of MCMB/Li simulation cell using (a) 1 M $LiClO_4$/PC and (b) 1 M $LiClO_4$/PC:BS (95:5 by volume) as electrolyte (i = 0.1 mA, cutoff is 2.00/0.005 V vs. Li/Li^+).

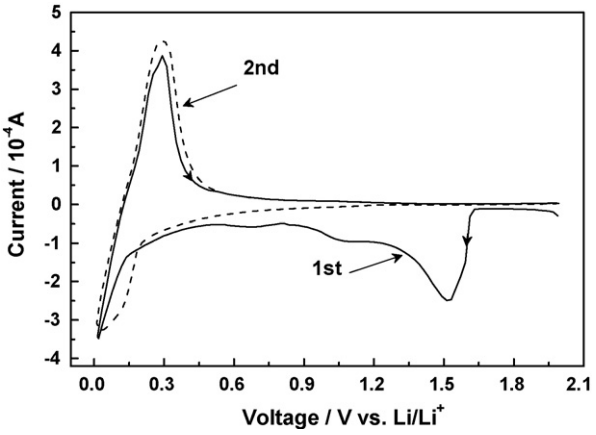

Fig. 5. Cyclic voltammograms of MCMB electrode in 1 M $LiClO_4$/PC:BS (95:5 by volume) with scan rate 0.1 mV s^{-1} at 25 °C.

voltage drops rapidly at the beginning, and then followed a discharge plateau in the voltage range of ca. 1.6–1.9 V. Below 0.2 V, Li^+ ions were intercalated into graphite. In the voltage range of 1.6–1.9 V, the decomposition of the electrolyte appeared on the graphite electrode. This resulted in formation of a passivating film on the graphite surface. This film is usually regarded as the SEI, which is ionically conductive and electronically insulating.

The decomposition processes of the BS additive are investigated by CV. Fig. 5 shows CV curves of MCMB electrode in 1 M $LiClO_4$ PC/BS (95:5 by volume). It can be observed that the obvious reductive current starts to appear at 1.6 V on the first cathodic sweep, which can be assigned to reductive decomposition of electrolyte solution to form surface film as discussed in the foregoing. In the second cycle, the peak at 1.6 V disappeared. The improvement of the electrochemical performance of graphite electrode is benefited from decomposition product of BS.

In Fig. 6(a), it can be obviously seen that the surface structure of graphite electrode is very clear-cut and much of interspaces between the MCMB particles is in existence before discharging. However, when the graphite electrode was discharged to 0.01 V, the surface of the graphite is well covered with passivating and compact film without any exfoliation. The great mass of the previous interspaces of the graphite electrode surface is filled in Fig. 6(b).

Ein-Eli et al. [7] demonstrated the feasibility of using sulfur dioxide (SO_2) gas as a passivating agent for the graphite anode which is in turn useful for Li ion rechargeable batteries. Based on the IR and XPS spectroscopy data, the studies indicated the reduction products of SO_2 comprised a mixture of Li_2S and Li-oxy-sulfur compounds (Li_2SO_3, $Li_2S_2O_4$ and $Li_2S_2O_5$), which are primarily responsible for the improved characteristics of the graphite anode upon repeated cycling. The primary theoretical studies focused on the SEI layer on a graphite electrode in the electrolyte system containing sulfite solvent [17]. The results showed that the compositions in SEI layer were mainly formed by a sulfite-type compound with an inorganic film like Li_2SO_3

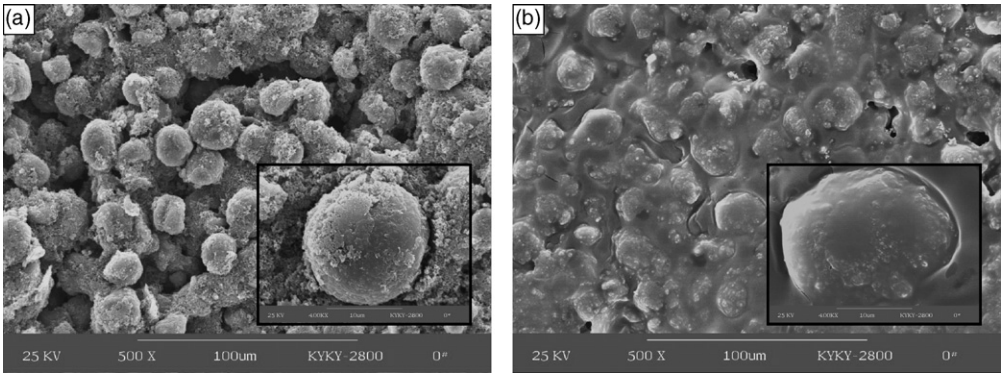

Fig. 6. SEM images of graphite electrode surface obtained (a) before discharge and (b) after the first discharge to 0.005 V in 1 M $LiClO_4$/PC:BS (95:5 by volume) electrolyte, Magnification ×500. (Inset) Magnification ×4000.

Table 2
Structural parameters (Å for bond lengths and degree for angles) for various carbonate and sulfite molecules

Parameter	BS	BC	PS	PC	ES	EC
C1–O2	1.467	1.471	1.470	1.472	1.462	1.460
O2–S3(C3)	1.740	1.379	1.752	1.378	1.742	1.383
S3(C3)–O4	1.733	1.379	1.747	1.382	1.761	1.383
O4–C5	1.474	1.471	1.457	1.457	1.457	1.460
C5–C1	1.544	1.544	1.531	1.546	1.525	1.535
S3(C3)═O6	1.486	1.205	1.490	1.204	1.490	1.203
C1–O2–S3(C3)	111.5	109.5	112.4	110.0	109.1	109.0
O2–S3(C3)–O4	91.7	110.4	91.2	110.3	91.1	110.2
S3(C3)–O4–C5	111.0	109.5	109.1	109.3	111.7	109.0
O2–S3(C3)–O6	105.9	124.8	106.3	125.0	111.2	124.9
O4–S3(C3)–O6	111.7	124.8	111.1	124.6	106.2	124.9

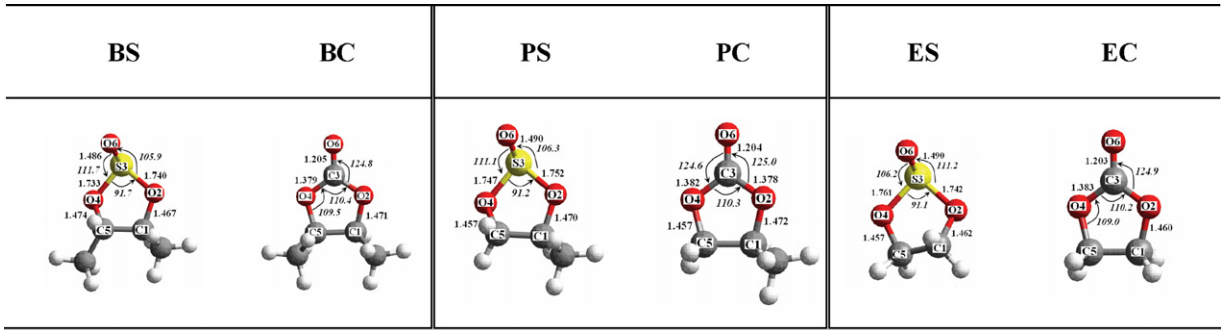

Fig. 7. Geometries optimized for various carbonate and sulfite molecules from BLYP/DNP.

Table 3
Total energy, frontier molecular orbital energy and dipole moment of various carbonate and sulfite molecules

Organic molecule	E_T (Ha)	Frontier molecular orbital energy (Ha)			dipole moment (Debye)
		E_{HOMO}	E_{LUMO}	ΔE_g [a]	
Butylene carbonate (BC)	−421.0941062	−0.2497	−0.0125	0.2372	5.9783
Propylene carbonate (PC)	−381.7839402	−0.2539	−0.0138	0.2401	5.6914
Ethylene carbonate (EC)	−342.4744144	−0.2575	−0.0183	0.2392	5.5066
Butylene sulfite (BS)	−781.1547869	−0.2489	−0.0748	0.1741	4.1979
Propylene sulfite (PS)	−741.8460885	−0.2526	−0.0793	0.1733	3.9628
Ethylene sulfite (ES)	−702.5371692	−0.2568	−0.0826	0.1742	3.6724

[a] $\Delta E_g = E_{LUMO} - E_{HOMO}$.

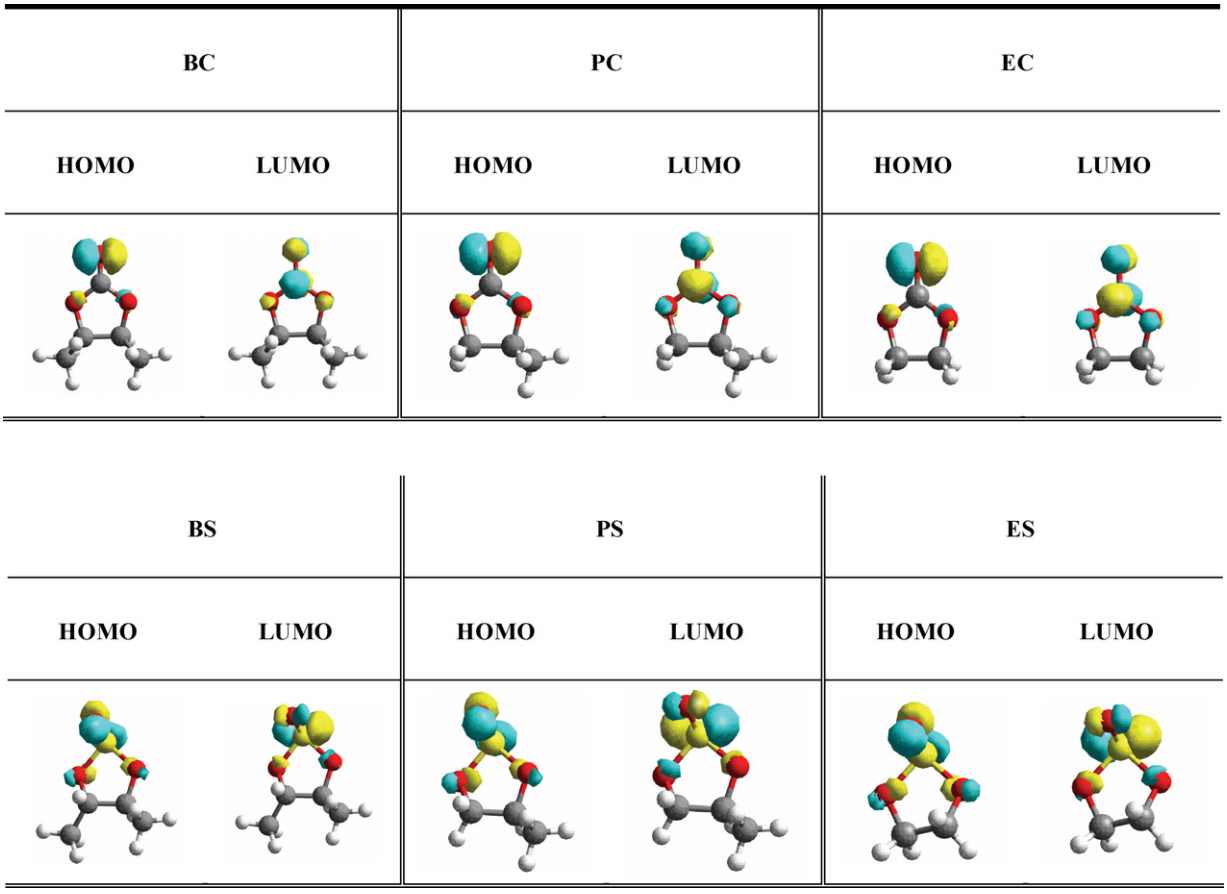

Fig. 8. Frontier molecular orbital of various cyclic carbonate and sulfite molecules.

and an organic one like $ROSO_2Li$. Relative theoretical studies focus on glycol sulfate (GS), ES, EC, PC, etc., indicated that these sulfites are more favorable to interaction with lithium atom than carbonate.

In order to understand these phenomena clearly, the molecular structures of cyclic carbonates and sulfites are optimized at the BLYP/DNP level. More information focus on the structural parameters for various organic molecules is summarized in Table 2. It can be considered that sulfite is formed by substitution S for C in $–CO_3$ radical of carbonate. The structure of sulfite exhibits very similarity to the carbonate seemingly, but there are essential differences between them in Fig. 7. The center atom of sulfite, S, is sp^3 hybridization. The $–SO_3$ radical is tetrahedral structure, and a lone-pair electron occupies one vertex of

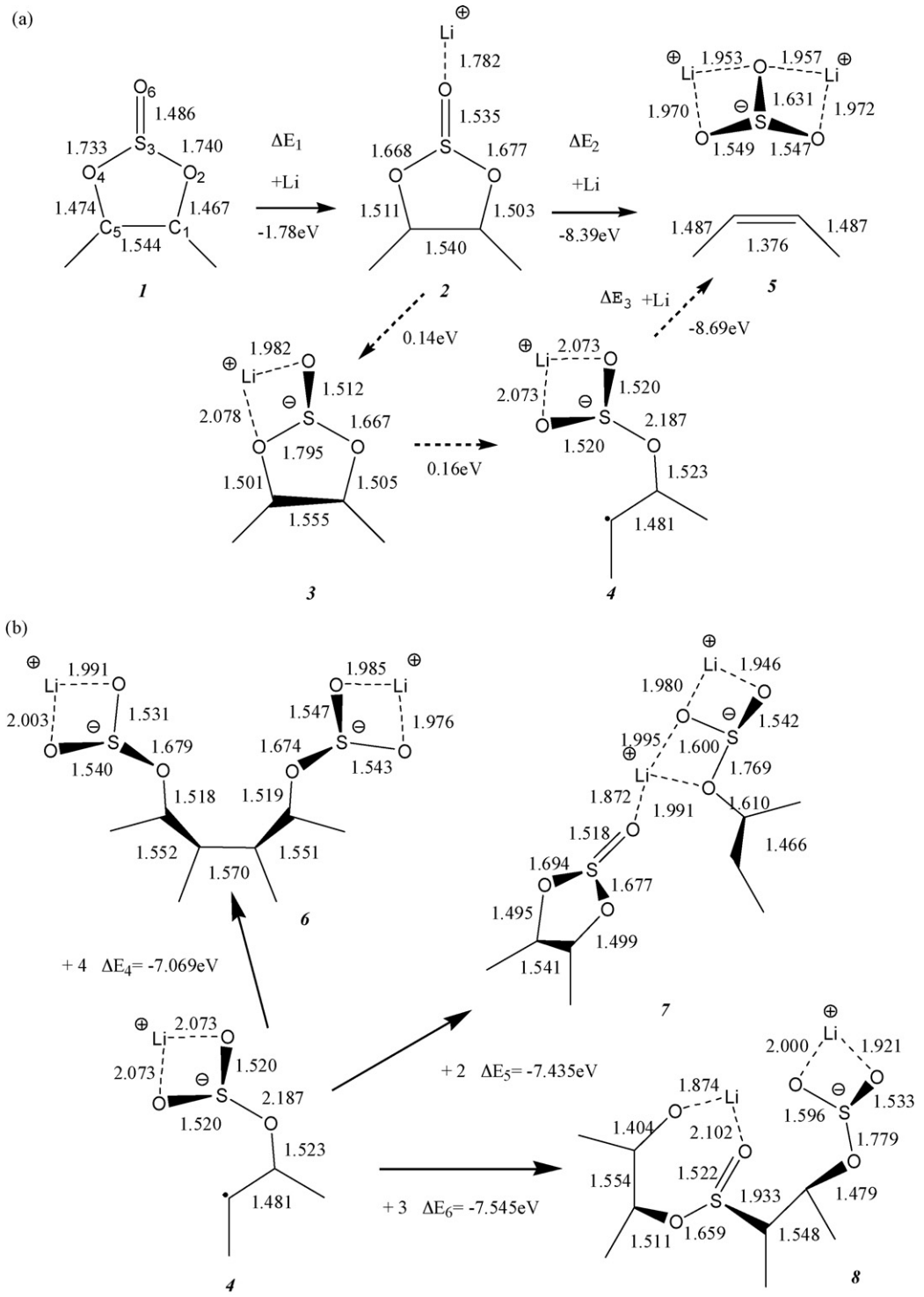

Fig. 9. The BLYP optimized geometries and (a) ΔE_1 and ΔE_2 values for the BS–Li_n complexes ($n = 0$, 1 and 2) and (b) Possible termination reactions of the radical anion 4 to form alkyl sulfide species. Units are in Å.

the tetrahedral structure. Furthermore, double bond of S and O is p^2–pd hybridization, which is different from that of carbonyl [24]. A σ bond is formed to overlap in axial direction of $3sp^3$ hybridization orbit of a lone-pair electron of S atom and $2p_x$ empty orbit of O atom. A π bond is formed to overlap in side direction of p orbit a lone-pair electron of O atom and 3d empty orbit of S atom, been called (d–p)π bond. This π bond has d orbit and can make electric charges on double bond disperse. Simultaneously, electron cloud density around O atom of double bond of S=O decreased, as well as its capability of losing electron, because of the action between two electronegativity O atoms and double bond of S=O. Therefore, the bond length of S=O of butylene sulfite (1.486 Å) is a little longer than that of C=O of butylene carbonate (1.205 Å) (Table 2). The relative electronegativity of $–SO_3$ radical (−0.658) is stronger than that of $–CO_3$ radical (−0.589).

Based upon the molecular orbital theory, the ability to gain and lose electrons is judged by the energy level of the highest occupied molecular orbital (HOMO) and the lowest unoccupied molecular orbital (LUMO) [25–27]. The total energy, the frontier molecular orbital energy, the energy gaps between the HOMO and LUMO, and the dipole moment of several cyclic carbonate and sulfite organic molecules are calculated and listed in Table 3. The LUMO energy and the total energy of the carbonate molecules are generally higher than that of the relevant sulfite molecules (shown in Fig. 8). It is clearly indicated that the organic sulfite molecules can easily accept electrons and bears a high reaction activity.

According to the above structure and bonding analysis on $–SO_3$ radical of sulfite organic molecules, Li^+ can coordinate with O atom of $–SO_3$ radical and then combine with solvent molecules. The optimized structures and binding energies (ΔE_1 and ΔE_2) of the lithium atoms in the BS–Li_n complexes ($n = 0$, 1 and 2) are shown in Fig. 9(a) together with some selected structural data. The ΔE_1 and ΔE_2 values are define as the energy changes in the stepwise addition reactions, BS + Li → BS–Li and BS–Li + Li → BS–Li_2, respectively. The reductive decomposition of BS initially encounters the ion-pair intermediates 2. An electron was transferred to BS in 2 to form the intermediate 3. The strong coordination between O atoms in $–SO_3$ radical of BS molecules and Li^+ results in the breaking up of five-member rings of BS molecules. And then, anion free radical builds up after Li^+(BS) gains an electron. As anion free radical is very likely and easier to undergo a reaction, compounds of butylene and $LiSO_3$ of the radical anion 4 are produced after it gains an electron. Then, Li_2SO_3 can be formed after these compounds share Li^+ of Li^+(BS). Studies indicated that the electrochemical performance can be improved obviously if Li_2SO_3 coated on the surface of graphite electrode. Therefore, we believe that the reason for the improved electrochemical performance of MCMB electrode with 1 M $LiClO_4$/PC:BS (95:5) electrolyte is that SEI films composed mainly of Li_2SO_3 on the surface of graphite electrode. Furthermore, it has been proven that the SEI layer on the graphite anode contained alkyl sulfide species [15,16].

Some possible termination ways of radical anion 4 to form alkyl sulfide species are shown in Fig. 9(b). The first termination way is the barrier-free self-dimerizing via nucleophilicly attacking the radical center by the another radical center to form 6, $(LiO_2SOCH(CH_3)CHCH_3)_2$. Additionally, of particular interest is the possibility of forming a species containing Li–O bonds solvated by a BS molecule, 7, LiO_2SO(Li–BS)$CH(CH_3)CHCH_3$, via electron-pairing between 4 and a reduction intermediate 2. The most probable reaction in Fig. 9(b) is that the combination of 4 with the reduction intermediate 3 also via electron-pairing generates a lithium organic salt with an ester group, 8, $LiOCH(CH_3)CH(CH_3)OS(O)CH(CH_3)CH(CH_3)OSO_2Li$, due to lowest Gibbs free energy of the reaction ($\Delta E_6 = -7.545$ eV).

During the last few years, manganese-based and iron-based oxides used as electrode materials in lithium ion batteries attracted lots of interests, owing to their favorable security and environmental benign [2,28]. In addition to the formation of passivating film on graphite anodes, the 1 M $LiClO_4$/PC:BS (95:5) electrolyte also allows the use of 4 V cathodes. The performance of charge/discharge of the first cycle and the 20 cycles for $LiMn_{1.99}Ce_{0.01}O_4$/Li and $LiFePO_4$-C/Li cell using 1 M $LiClO_4$/PC:BS (95:5 by volume) as electrolyte are showed in Figs. 10 and 11, respectively. The results indicate that the PC/BS electrolyte has a high oxidation stability allowing the cycling of a $LiMn_{1.99}Ce_{0.01}O_4$ and $LiFePO_4$-C cathodes with good reversibility.

Figs. 12 and 13 show the cycle voltammogram for the $LiMn_{1.99}Ce_{0.01}O_4$ and the $LiFePO_4$-C electrodes in 1M $LiClO_4$/PC:BS (95:5) electrolyte, respectively. It can be found that the oxidation potential of the electrolyte is as high as 4.5 V

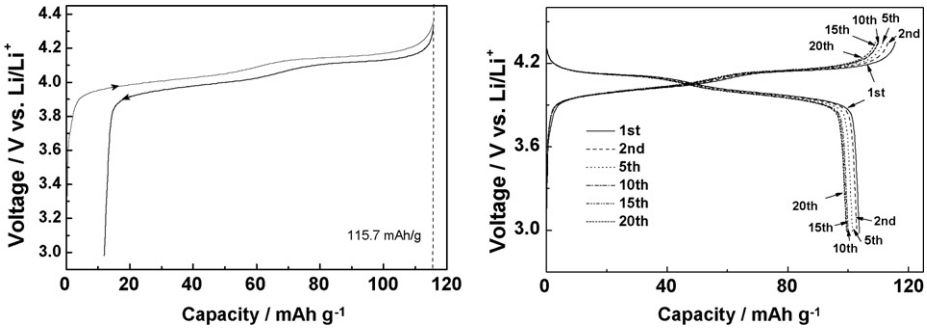

Fig. 10. The charge/discharge curves of the first cycle (a) and the first 20th cycles (b) for $LiMn_{1.99}Ce_{0.01}O_4$/Li cell using 1 M $LiClO_4$/PC:BS (95:5 by volume) as electrolyte ($i = 0.1$ mA, cutoff at 4.35/3.00 V vs. Li/Li^+).

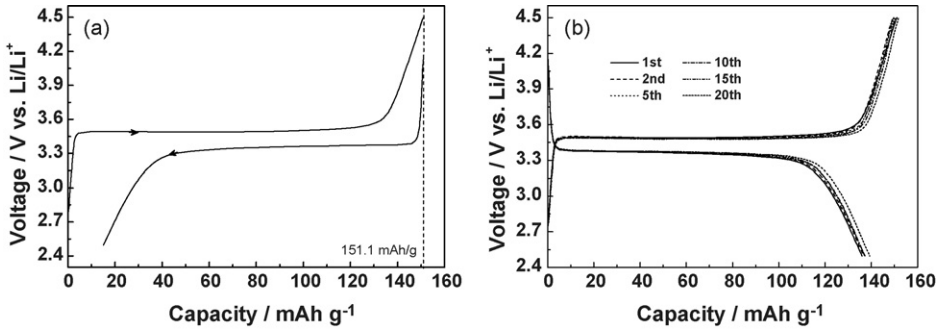

Fig. 11. The charge/discharge curves of the first cycle (a) and the first 20th cycles (b) for $LiFePO_4$-C/Li cell using 1 M $LiClO_4$/PC:BS (95:5 by volume) as electrolyte ($i = 0.1$ mA, cutoff at 4.5/2.5 V vs. Li/Li^+).

versus Li/Li^+. The oxidation peaks at about 4.04 and 4.15 V corresponding to the charge plateaus and the reductive peaks at about 3.93 and 4.06 V corresponding with the discharge plateaus are shown in Fig. 12. The oxidation peak at 3.5 V and the reductive peak at 3.3 V relates to the charge and discharge plateaus in Fig. 13, respectively.

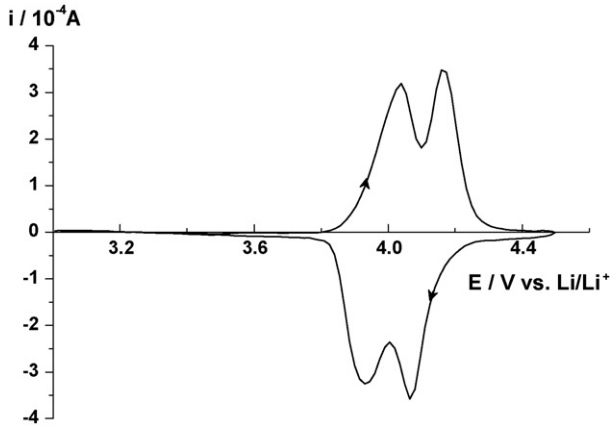

Fig. 12. Cycle voltammogram of $LiMn_{1.99}Ce_{0.01}O_4$ electrode in 1 M $LiClO_4$/PC:BS (95:5 by volume) with scan rate 0.1 mV s^{-1} at 25 °C.

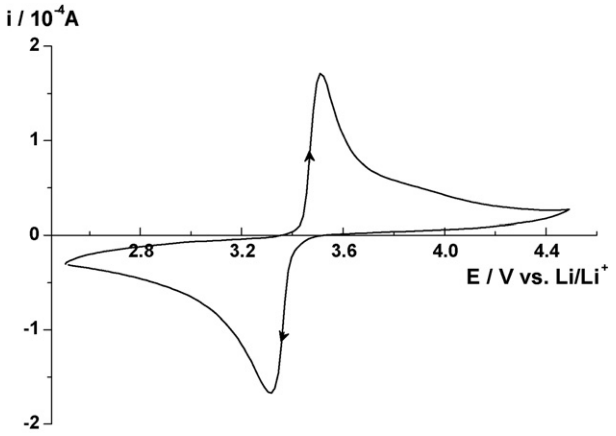

Fig. 13. Cycle voltammogram of $LiFePO_4$-C electrode in 1M $LiClO_4$/PC:BS (95:5 by volume) with scan rate 0.1 mV s^{-1} at 25 °C.

4. Conclusion

A new liquid electrolyte containing butylene sulfite (BS) and PC has been investigated for use in lithium ion batteries with advantageous thermal stability and electrochemical performance. BS exhibits promising characteristics as a film-forming electrolyte additive in lithium ion batteries. A small amount of BS (5 vol.%) can effectively prevent the co-intercalation of PC with solvation lithium ion into graphite. The formation of a compact and stable SEI film on the graphite flake surface is believed to be the reason for the improved cell performance. The total energy and the frontier molecular orbital energy of several cyclic organic carbonate and sulfite molecules are studied by the DFT calculations. The LUMO energy and the total energy of the carbonate molecules are higher than that of the sulfite molecules. It is clearly indicated that the sulfites can easily accept electrons and bears a high reaction activity. The reductive decomposition of BS initially encounters an ion-pair intermediate and then cleavages homolytically to generate a radical anion. It will undergo secondary reactions by further reduction, ion-pairing (Li_2SO_3), probably barrier-free self-dimerizing ($(LiO_2SOCH(CH_3)CHCH_3)_2$), and electron-pairing ($LiO_2SO(Li–BS)CH(CH_3)CHCH_3$ and $LiOCH(CH_3)CH(CH_3)OS(O)CH(CH_3)–CH(CH_3)OSO_2Li$) processes. The lithium-oxy-sulfite film (Li_2SO_3 and $ROSO_2Li$) is beneficial to improve the electrochemical performance when it coated on the surface of graphite electrode. In addition, the PC/BS electrolyte has been proved to have a high anti-oxidation ability allowing the cycling of the $LiMn_{1.99}Ce_{0.01}O_4$ and $LiFePO_4$-C cathodes with good reversibility.

Acknowledgments

This work was financially supported by the National 973 Program (Contract no. 2002CB211800), the National Key Program for Basic Research of China (Contract no. 2001CCA05000) and 863 Program (Contract no. 2005AA501620). The authors thank Prof. C.M. Hong (College of Chemistry and Molecular Engineering, Peking University) for his critical reading to this manuscript and Prof. H.L. Luan (Beijing General Research Institute of Mining and Metallurgy) for synthesize of butylene sulfite assistance. The authors are grateful to 3M Company for providing the LiTFSI sample.

References

[1] K. Xu, Chem. Rev. 104 (2004) 4303.
[2] M.S. Whittingham, Chem. Rev. 104 (2004) 4271.
[3] R. Oesten, U. Heider, M. Schmidt, Solid State Ionics 148 (2002) 391.
[4] J. Arai, H. Katayama, H. Akahoshi, J. Electrochem. Soc. 149 (2002) A217.
[5] M. Winter, J.O. Besenhard, M.E. Spahr, P. Novak, Adv. Mater. 10 (1998) 725.
[6] J.O. Besenhare, P. Castella, M.W. Wagner, Mater. Sci. Forum 91–93 (1992) 647.
[7] Y. Ein-Eli, S.R. Thomas, V.R. Koch, J. Electrochem. Soc. 144 (1997) 1159.
[8] A. Naji, J. Ghanbaja, P. Willmann, D. Billaud, Electrochim. Acta 45 (2000) 1893.
[9] Z.X. Shu, R.S. McMillan, J.J. Murray, I.J. Davidson, J. Electrochem. Soc. 142 (1997) L161.
[10] Y.S. Hu, W.H. Kong, H. Li, X.J. Huang, L.Q. Chen, Electrochem. Commun. 6 (2004) 126.
[11] Y.S. Hu, W.H. Kongm, Z.X. Wang, H. Li, X.J. Huang, Electrochem. Solid-State Lett. 7 (2004) A442.
[12] G.H. Wrodnigg, J.O. Besenhare, M. Winter, J. Electrochem. Soc. 146 (1999) 470.
[13] G.H. Wrodnigg, T.M. Wrodnigg, J.O. Besenhard, M. Winter, Electrochem. Commun. 1 (1999) 148.
[14] G.H. Wrodnigg, J.O. Besenhard, M. Winter, J. Power Sources 97–98 (2001) 592.
[15] H. Ota, T. Sato, H. Suzuki, T. Usami, J. Power Sources 97–98 (2001) 107.
[16] H. Ota, T. Akai, H. Namita, S. Yamaguchi, M. Nomura, J. Power Sources 119–121 (2003) 567.
[17] Y.K. Han, S.U. Lee, J.H. Ok, J.J. Cho, H.J. Kim, Chem. Phys. Lett. 360 (2002) 359.
[18] H.H. Zheng, K. Jiang, T. Abe, Z. Ogumi, Carbon 44 (2006) 203.
[19] M. Itagaki, N. Kobari, S. Yotsuda, K. Watanabe, S. Kinoshita, M. Ue, J. Power Sources 148 (2005) 78.
[20] H.S. Byun, L. He, R. Bittman, Tetrahed. 56 (2000) 7051.
[21] B.B. Lohray, Synthesis (1992) 1035.
[22] B.M. Kin, K.B. Shaipless, Tetrahed. Lett. 30 (1989) 655.
[23] DMol User Guide, Biosym/MSI, San Diego, 1995, pp E-2–E-4.
[24] J.G. Pritchard, P.C. Lauterbur, J. Am. Chem. Soc. 83 (1961) 2105.
[25] Y. Matsuo, K. Fumita, T. Fukutsuka, Y. Sugie, H. Koyama, K. Inoue, J. Power Sources 119 (2003) 373.
[26] H. Yoshitake, K. Abe, T. Kitakura, J.B. Gong, Y.S. Lee, H. Nakanmura, M. Yoshio, Chem. Lett. 32 (2003) 134.
[27] P. Ghimire, H. Nakamura, M. Yoshio, H. Yoshitake, K. Abe, Chem. Lett. 34 (2005) 1052.
[28] J.B. Goodenough, Lithium Ion Batteries: Fundamentals and Performance, John Wiley & Sons, Inc., New York, 1998.